10TH INTERNATIONAL SYMPOSIUM ON PARTICLE IMAGE VELOCIMETRY – PIV13
Delft, The Netherlands, July 2-4, 2013

Simultaneous 3D PTV and infrared tomographic PIV measurement of zooplankton distribution in unsteady flow fields

Deepak Adhikari[1], Michael Hallberg[1] and Ellen Longmire[1]

[1] Department of Aerospace Engineering and Mechanics, University of Minnesota, Minnesota, USA
adhi0018@umn.edu

ABSTRACT
Copepods and brine shrimp, which represent different species of zooplankton with similar inertial time constant, can behave very differently when subjected to velocity gradients in unsteady or turbulent flows. Upon sensing hydrodynamic disturbances, copepods can respond with rapid acceleration and high speed. Brine shrimp, on the other hand are more passive and capable of only small relative swimming speeds. A goal of the current study is to understand copepod response thresholds and their effect on copepod number distribution in complex flows. We describe a simultaneous 3D PTV and infrared tomographic PIV measurement system as a means to obtain volumetric flow fields and three-dimensional tracks of zooplankton within a volume. A tomographic PIV measurement volume was illuminated with an Oxford Firefly infrared laser (wavelength: 808 nm) and viewed by four high-speed cameras (1280 × 800 pixels) fitted with infrared pass optical filters. The infrared pass filters are needed to allow only the infrared illumination scattered from the seed particles to pass through the lens. The 3D PTV system included two white LED lamps placed in a dark-field illumination configuration, and two additional high-speed cameras (1280 × 800 pixels) fitted with infrared-blocking optical filters. The LED lamps and infrared-blocking filters were effective at illuminating the zooplankton but not the tracer particles. Experiments were carried out in a re-circulating seawater channel driven by a paddlewheel. The paddlewheel ensures that zooplanktons in the seawater are not damaged. We present results of brine shrimp and copepod distributions ahead of and behind a cylinder in crossflow with Re = 930. The number distributions are compared with distributions of principal strain rate of the flow at the position of each zooplankton, and the results are assessed. While brine shrimp exhibit uniform distributions across the cylinder wake, the distribution of copepods shows a deficit directly behind the cylinder. This difference in distribution is attributed not to local strain in the wake, but instead to escape responses of copepods upstream of the cylinder due to sudden decelerations.

1. INTRODUCTION

Zooplankton generally drift with large eddies (~kilometers) in the ocean, but they may move independently of smaller eddies (~millimeters to centimeters). For instance, copepods, with swimming speeds substantially higher than small-scale fluctuation velocities, can exhibit motion independent of the surrounding flow [1]. Generally, copepods can detect sudden flow perturbations that trigger them to swim at speeds of up to 0.5 m/s. By contrast, brine shrimp, which are capable of only low swimming speeds (~3 mm/s), effectively move passively with the local fluid velocity [2]. This suggests that distributions of different zooplankton species may vary depending on the flow conditions and scales. Modeling such distributions requires understanding unique locomotion and sensory attributes of the individual species.

Copepods use their setae to sense flow disturbances and elicit high speed escape responses [3,4]. This flow disturbance refers mainly to local fluid velocity gradients, since the gradients promote differences in velocity near individual setae. Kiørboe et al (1999) [5] subdivided velocity gradients into vorticity, normal strain, shear strain, and acceleration and subjected copepods to different flows exhibiting these conditions. Based on a simplified model, they determined a threshold for either normal or shear strain of 0.4 s^{-1} as being the minimum required for copepod escape response. In a later work, particle image velocimetry (PIV) was used in shear dominated flow, and the results showed that copepods could respond to shear rates as low as 0.025s^{-1} [6]. More recently, high resolution PIV and volumetric PIV have been used to understand the propulsion of copepods [7, 8, 9].

Previous work has shown that interaction between turbulent fluid and zooplankton motions can be highly coupled, complex and three-dimensional. For better insight into their interaction, a measurement system needs to be capable of measuring both flow velocity and zooplankton motion in three-dimensions and at high repetition rate. The purpose of the present work is to demonstrate a novel volumetric velocimetry and tracking system capable of quantifying zooplankton and turbulent fluid motion simultaneously and instantaneously. In this paper, we study the behavior and distribution of the two zooplankton types within the wake of a vertically mounted cylinder.

2. FACILITY AND MEASUREMENT TECHNIQUE

2.1 Water Channel Facility

A recirculating seawater channel facility with a uniform cross section was used (see figure 1). The channel was fitted with a paddlewheel that was driven by a high-torque permanent magnet gear motor with closed-loop feedback motor controller (Dart Model PU-40E). The paddlewheel was used to drive the flow in order to avoid damaging the mechanoreceptors (setae) and oars of the zooplankton when they are added to the fluid. The width of the channel was 150 mm, and seawater was filled to a height of 150 mm. Honeycombs and screens were mounted in the channel as flow conditioners, and the test section was 1.3 meters downstream. Seawater was obtained from a pipeline connected to the Gulf of Mexico. The water was passed through a 2 µm filter before filling up the channel.

The free stream velocity was maintained at U_0 = 0.077m/s. The cylinder, with diameter d_c = 12.7 mm and height h_c = 300 mm, was placed just upstream of the test section to perturb the flow. The Reynolds number based on the cylinder diameter was Re_d = 930. The channel was seeded with 55µm titanium dioxide-filled polyamide tracer particles, and zooplanktons were distributed throughout the fluid. The seeding particles do not harm the zooplankton, and they scatter infrared illumination for tomographic PIV effectively.

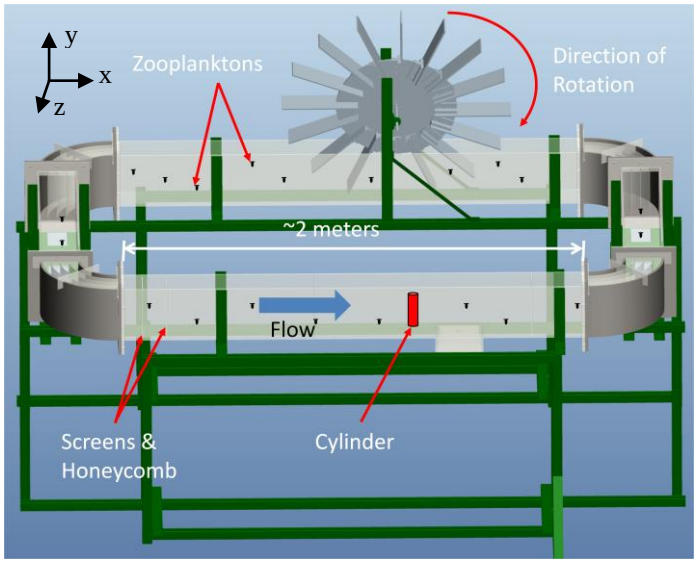

Figure 1 Schematic diagram of the aquatic flow facility, driven by paddle wheel.

2.2 Species

The zooplankton species examined were copepods (size ~ 1 mm) and brine shrimp (size ~ 1 mm), such that experiments for each species were carried out independently.

The copepods (*Acartia tonsa*) were collected from Mustang Island, Texas (27°48′N, 97°05′W). In order to ensure that only one species of copepod was used for the experiment, the collected water sample was first passed through a 4000 µm mesh to filter off bigger plants and organisms. Next, the filtered sample was passed through a 150 µm mesh to remove smaller planktons. Finally, a point source light was used to attract the copepods to one end of a container before they were captured and transferred to the water channel.

The brine shrimp (*Artemia salina*) were cultured in the laboratory. Brine shrimp eggs were placed in a hatchery. After 2 days, a point light source was used to attract them and contain them before they were transferred to the water channel.

2.3 3D PTV and Infrared Tomographic PIV Setup

Simultaneous infrared tomographic PIV [10] and 3D particle tracking velocimetry (3D PTV) [11] were applied to measure fluid motion and zooplankton distribution (see figure 2). The tomographic PIV measured volumetric velocity variation within the fluid, while the 3D PTV tracked the zooplankton independently. For tomographic PIV, the measurement volume was illuminated with an Oxford Firefly infrared laser (wavelength: 808 nm) with 3 mJ/pulse and pulse duration of 10 µs. The beam was expanded into a sheet with thickness ~20 mm. Four high-speed cameras (1280 × 800 pixels), fitted with infrared pass optical filters, were mounted and aimed at the measurement volume. The infrared pass filters were needed to allow only the infrared illumination scattered from the seed particles to pass through the lens. Simultaneously, for 3D PTV, the measurement volume was illuminated with two white LED lamps placed in a dark-field illumination configuration. Two additional high speed cameras (1280 × 800 pixels), fitted with infrared-

blocking optical filters, were aimed at the measurement volume to image the zooplankton. The LED lamps and infrared-blocking filters were effective at illuminating the zooplankton but not the tracer particles. Typical images acquired for tomographic PIV and 3D PTV is represented in figure 3(a) and (b), respectively. Figure 3(a) shows mainly the tracer particles, while figure 3(b) shows zooplankton (brine shrimp) within the flow. These images successfully demonstrate the use of the current experimental arrangement to segment the zooplankton from the tracer particles using cameras and optical filters.

A calibration plate was traversed to nine positions spanning the depth of the measurement volume, and a preliminary mapping function was determined from the resulting camera images. A self-calibration procedure reduced disparity errors and hence corrected the calibration mapping function for all cameras leading to a reduced calibration error [12]. For tomographic PIV, particle intensity volumes were reconstructed using the MLOS-SMART algorithm implemented in DaVis 8.0. The recordings in all cameras were synchronized with the laser pulse frequency at 130 fps. This provided a time series with frames separated by $\Delta t = 7.7$ ms. The size of the measurement volume was -40 mm < x < 40mm, -32 mm < y < 7.5 mm and 0 mm < z < 19 mm. It is noted that zooplanktons may be visible in figure 3(a); thus, mask was applied on the reconstructed volume to remove any zooplankton that may contaminate the local flow velocity vectors during cross-correlation. The interrogated fluid volume was masked at locations where zooplanktons were present with a cubic mask of 7 × 7 × 7 voxels. Masking was carried out to avoid contamination of fluid vectors near the zooplankton. Cross-correlating masked volume pairs separated by Δt obtained velocity fields. The smallest interrogation volume yielding high quality results was 48 × 48 × 48 voxels, providing a vector resolution in all three directions of 3.65mm. Using a 75% overlap resulted in fields of 88 × 43 × 21 vectors. For 3D PTV, the zooplankton organisms were identified automatically in individual images using an image processing routine for zooplankton segmentation. The routine resulted in a binary image with the location of each organism represented by a 3 × 3 pixel area of high intensity value. A 3D PTV operation in DaVis 8.0 was then applied to locate the position of each zooplankton in the three-dimensional volume and to measure its velocity. The resulting vector fields from the tomographic PIV operation and the tracks from the 3D PTV were combined into Tecplot for analysis.

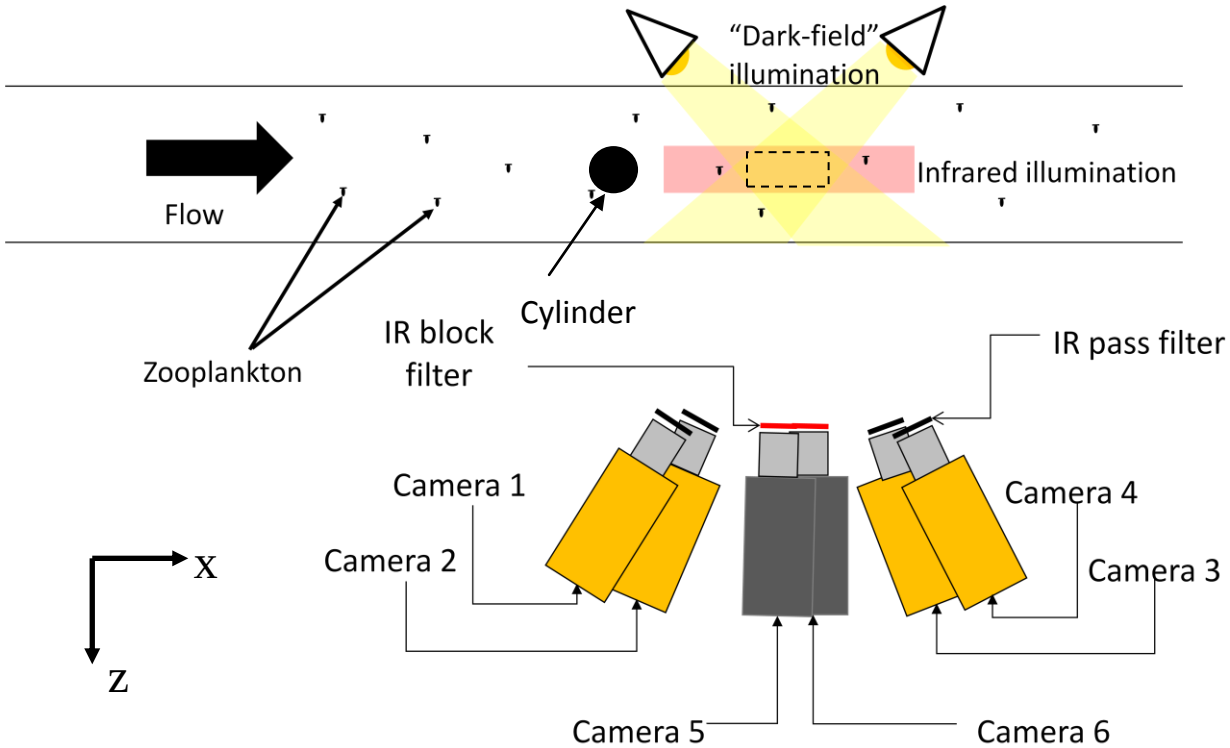

Figure 2 Schematic view of the simultaneous tomographic PIV (cameras 1, 2, 3, 4) and 3D PTV measurement system (cameras 5, 6) to measure instantaneous flow field and location of the copepods in a volume. Dashed box within the infrared illumination represents the measurement volume.

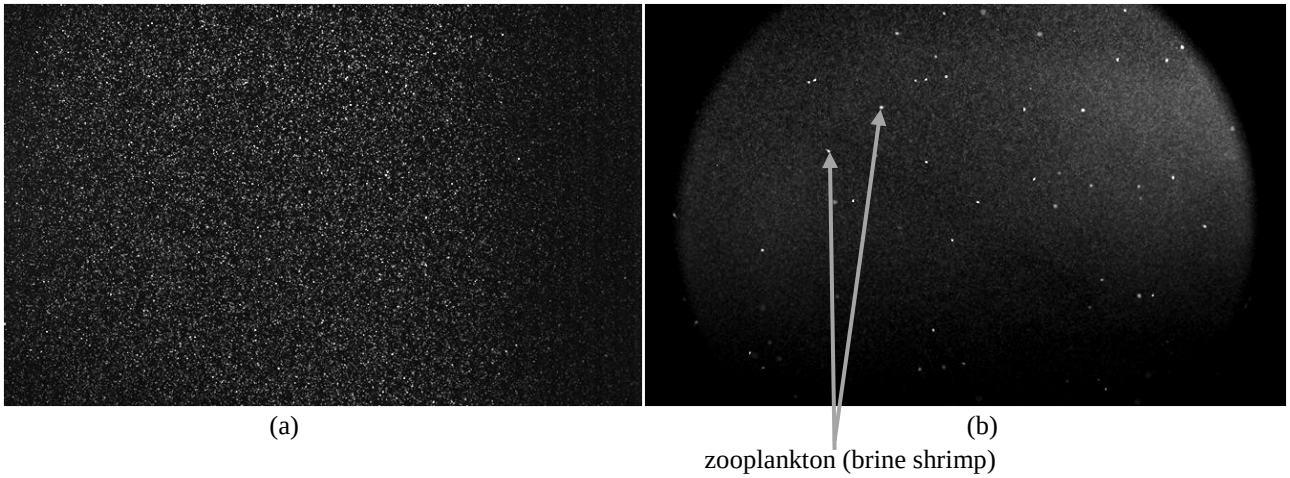

Figure 3 Typical image obtained for (a) tomographic PIV (camera 4) and (b) 3D PTV (camera 5). Images were taken at the same time instance.

3. DERIVING FLOW QUANTITIES

3.1 Velocity Gradient

Since 3D PTV locates the position of the zooplankton exactly, while PIV obtains velocity values in a pre-defined structured grid, a coincident zooplankton location and grid point location is highly unlikely. Therefore, interpolation of flow quantities at the zooplankton location is needed to obtain the local flow velocity and its gradients. We consider the neighboring grid points (64 points) of the zooplankton location, and apply a Taylor-series least-square technique [13] to obtain both the velocity of the fluid and the spatial velocity gradients, simultaneously.

3.2 Maximum Principal Strain

Quantifying the strength of local deformation rates from the velocity gradients is dependent on the coordinate system. Since the copepods are aligned at arbitrary angles to the Cartesian coordinates when sensing fluid disturbances, maximum principal strain was used to determine the hydrodynamic disturbance independent of the copepod orientation [7].

The maximum principal strain was calculated by finding the eigenvalues of the symmetric component of the complete velocity gradient tensor (also known as strain rate tensor):

$$e_{ij} = \begin{bmatrix} \frac{\partial u}{\partial x} & \frac{1}{2}\left(\frac{\partial u}{\partial y}+\frac{\partial v}{\partial x}\right) & \frac{1}{2}\left(\frac{\partial u}{\partial z}+\frac{\partial w}{\partial x}\right) \\ \frac{1}{2}\left(\frac{\partial u}{\partial y}+\frac{\partial v}{\partial x}\right) & \frac{\partial v}{\partial y} & \frac{1}{2}\left(\frac{\partial v}{\partial z}+\frac{\partial w}{\partial y}\right) \\ \frac{1}{2}\left(\frac{\partial u}{\partial z}+\frac{\partial w}{\partial x}\right) & \frac{1}{2}\left(\frac{\partial v}{\partial z}+\frac{\partial w}{\partial y}\right) & \frac{\partial w}{\partial z} \end{bmatrix} \quad (1)$$

where u, v, w are the velocity components in the orthonormal x, y, z directions, and

$$det\left(e_{ij} - \lambda_k \delta_{ij}\right) = 0. \quad (2)$$

In equation (2), *det* refers to the determinant of the tensor, δ_{ij} is the Kronecker delta tensor, and and λ_k (k = 1, 2, 3) represent the eigenvalues, or principal strain rates. The maximum principal strain rate is then obtained as $\lambda_{max} = max(|\lambda_1|, |\lambda_2|, |\lambda_3|)$.

3.3 Uncertainty Estimation

The measured uncertainty in the spatial derivatives can be ascertained using the mass conservation principal [14]. Figure 4 shows the divergence of the velocity at 64000 coordinates (randomly selected) within each measurement domain for all the independent data sets of flow behind the mounted cylinder. The statistical distribution of the divergence estimated by the Taylor-series least-square interpolation results in a fitted Gaussian curve centered at zero with a width of 0.04. Adrian and Westerweel [15] estimated a relative error distribution for all voxels that can be expressed as

$$\overline{\left(\frac{\partial u}{\partial x}+\frac{\partial v}{\partial y}+\frac{\partial w}{\partial z}\right)^2} \cong \left(\frac{\sigma_{\Delta x}}{D_I \Delta t}\right)^2 \quad (3)$$

where $\sigma_{\Delta x}$ is the overall error amplitude of the displacement, D_I is the dimension of non-overlapping interrogation domain in the cross-correlation procedure, and Δt is the time delay between two consecutive frames. Using equation (3), the uncertainty of displacement, $\sigma_{\Delta x}$, is given as 0.3 voxels, which implies uncertainty of an individual flow field vector as 0.003m/s ($\sim 0.04U_0$).

For 3D PTV, the uncertainty of the zooplankton location is estimated to be within 2 voxels (or 0.15 mm). Thus, the velocity error was estimated to be 0.02 m/s ($\sim 0.3U_0$) if consecutive images are used.

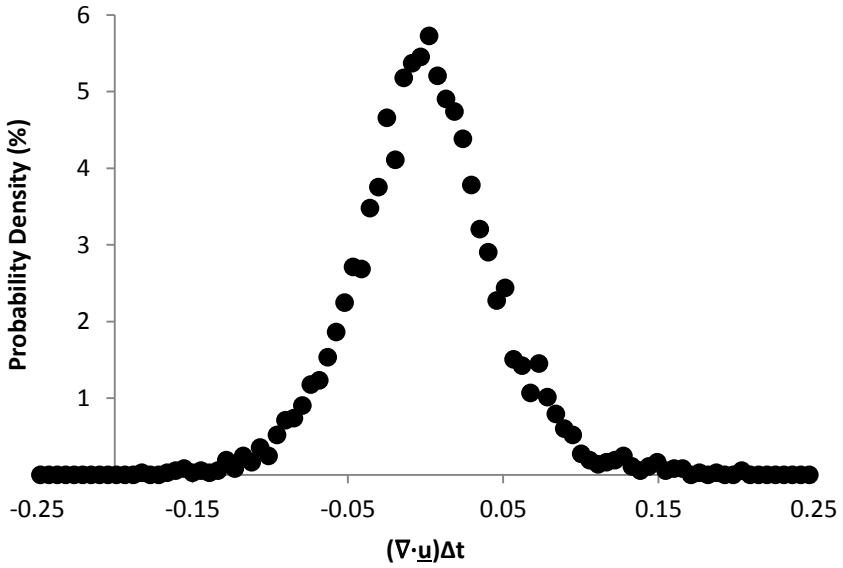

Figure 4 Probability density function of the relative error distribution of the flow field behind the mounted cylinder.

4. RESULTS

Figure 5 shows a sample of an instantaneous copepod distribution behind the cylinder. The flow is moving in the positive x-direction. The volumetric field includes an iso-surface of vorticity magnitude ($\|\omega\| = 25\ s^{-1}$) with contour colors representing total velocity magnitude. Red spheres represent copepods. The figure highlights the capability of this technique to obtain the entire volumetric flow field and the distribution of the zooplankton within the field simultaneously. Copepod jumps can be observed and quantified from neighboring time steps in the series.

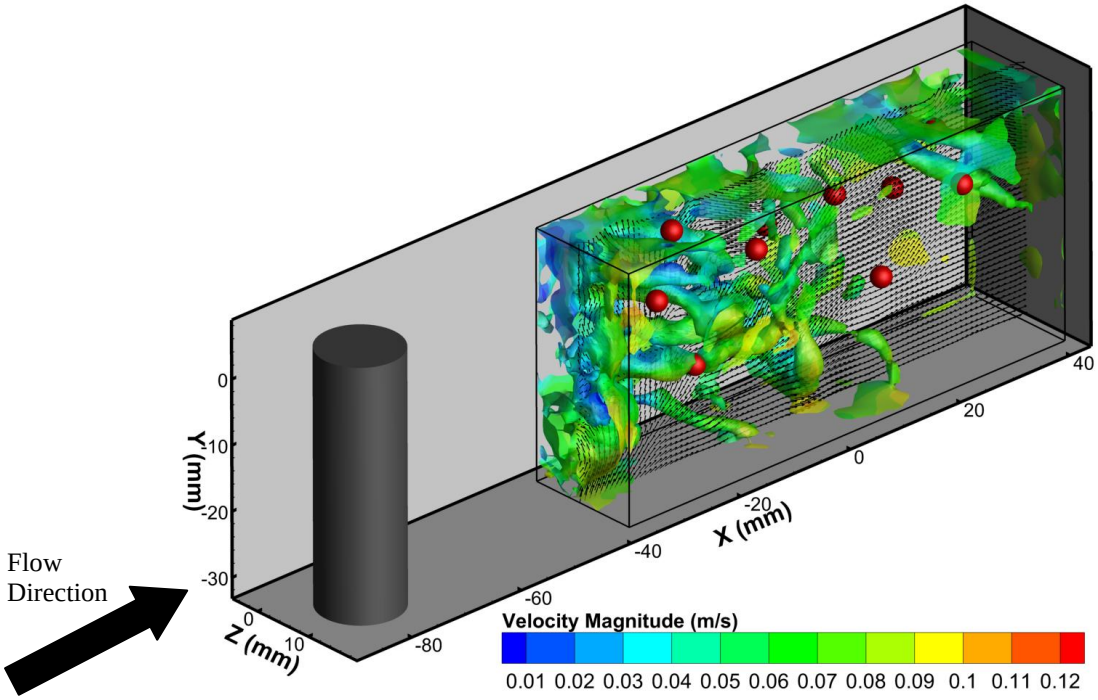

Figure 5 Volumetric flow field and copepod distribution behind a vertically mounted cylinder located at x = -80 mm, z = 9.5mm. Height of the cylinder has been truncated for clarity. The vorticity iso-surface is $||\omega|| = 25\ s^{-1}$.

The inertial Stokes number for both copepod and brine shrimp (when not actively moving) was estimated as $Sk \sim 0.3$ with respect to the largest estimated eddy behind the cylinder. Without active motion, both zooplankton are therefore influenced in a similar manner by eddies. The Stokes number is given as:

$$Sk = \frac{\tau_p}{\tau_f}\ ; \tau_p = \frac{(\rho_p - \rho_f){d_p}^2}{18\rho_f \nu_f};\ \tau_f = \frac{d_c}{U_0}, \tag{4}$$

where ρ_p is the density of the zooplankton, ρ_f is the density of the fluid, d_p is the length of the zooplankton, ν_f is the kinematic viscosity of the fluid, d_c is the diameter of the cylinder and U_0 is the free stream velocity.

Stokes numbers based on smaller eddies would obviously be larger. Thus, although *Sk* is comparable for both species neither copepods nor brine shrimp are expected to track the smaller eddy motions faithfully (as would the tracer particles Sk <<1). On the other hand their passive motions can be influenced significantly by the largest eddies. However, when a copepod senses certain local velocity gradient characteristics, it can respond actively with high acceleration and slip velocity (order of magnitude higher than U_0). Thus, the spatial distribution of copepods downstream of the cylinder may differ from that of the brine shrimp.

4.1 Downstream of cylinder

Measurements were taken at three different locations in the z-direction: (1) measurement volume directly behind the cylinder (as shown in figure 5), (2) volume offset from cylinder axis by 1.5cm in positive z-direction, and (3) volume offset from cylinder axis by 3.0 cm in positive z-direction. Independent realizations of data were sampled from time series image sequences. For both brine shrimp and copepods, 495 independent fields were obtained. From the image sets, the positions of all the zooplankton were recorded.

Figure 6 shows graphs of total zooplankton count against z-direction based on all of the independent data sets. There were different numbers of brine shrimp (4916) and copepods (9215) counted within the datasets. Thus, for better comparison, the count was normalized using the average number of each zooplankton across the z-direction. From figure 6(a) the brine shrimp appear to be distributed evenly across the z-direction even with the presence of the cylinder. However, there are ~14% fewer copepods (figure 6b) present directly behind the cylinder as compared to away from the cylinder. This could be due to strong velocity gradients either upstream of the cylinder or downstream in the wake of the cylinder. In order to gain a better understanding, we look at the maximum principal strain at zooplankton locations downstream of the cylinder.

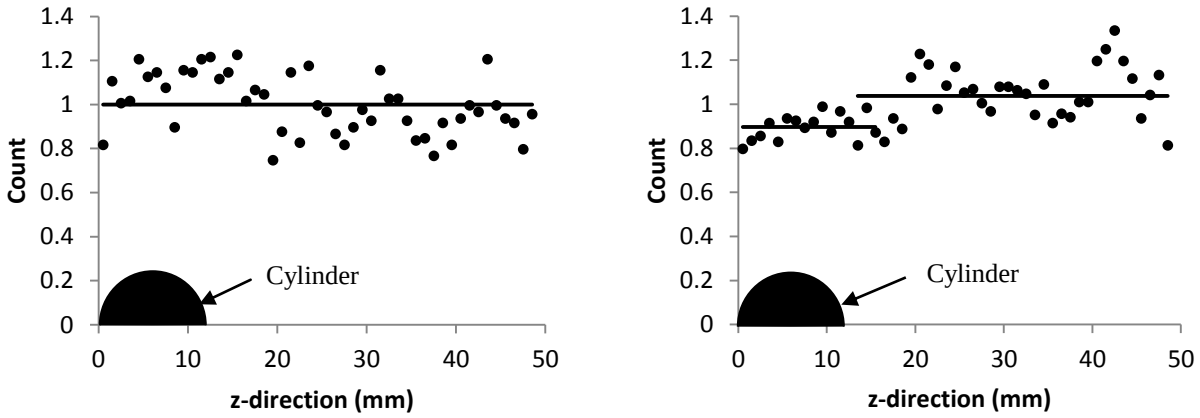

(a) (b)

Figure 6 Zooplankton count against z-direction for (a) brine shrimp and (b) copepods. The count has been normalized with the average value of the respective zooplankton for clarity in comparison. Counts at each z location include all x and y locations within the field of view.

Figure 7 shows the distribution of local maximum principal strain rate directly behind the cylinder (z = 0 mm to 15 mm) at the location of the zooplankton for each species. From the figure, the distributions of both brine shrimp and copepod are similar, and the value ranges from 0 to ~25 s^{-1} with a peak at ~8 s^{-1}. Almost the entire distribution is higher than ~0.4 s^{-1} and ~0.025s^{-1}, the threshold quantities measured by [5] and [6], respectively. Even higher principal strains (> 25 s^{-1}) caused by smaller eddies (< ~3 mm) may be present in the flow. However, they do not appear in the graph due to the finite spatial resolution of tomographic PIV. From figure 7, copepods appear to stay within these high strain rate regions rather than move toward lower strain regions. The time series video acquired for 3D PTV also shows that very few of the copepods exhibited jumps while in the wake of the cylinder. This suggests that the principal strain rate downstream of the cylinder might not be responsible for the uneven distribution of copepod shown in figure 6. Thus, the cause of the uneven distribution likely results from their behavior upstream of the cylinder.

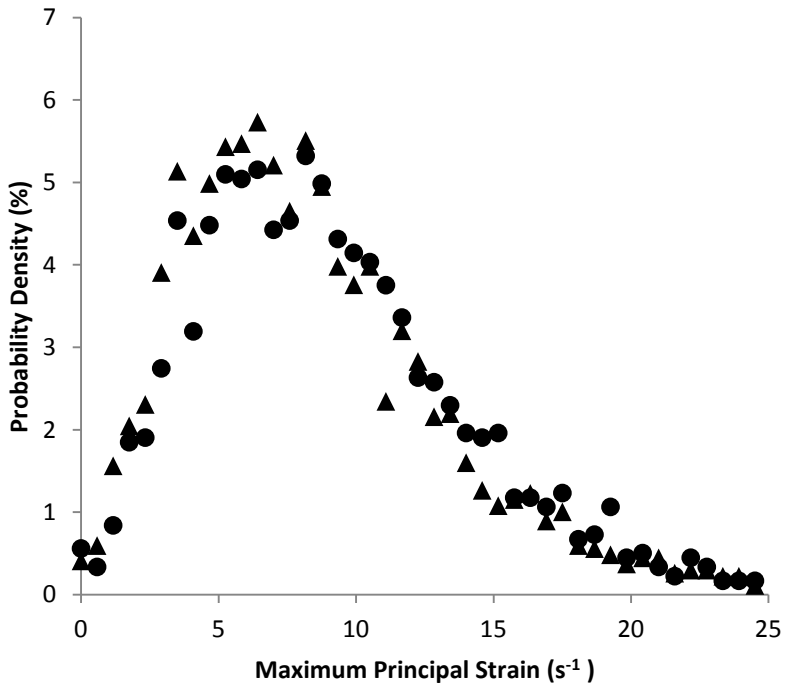

Figure 7 Probability density functions of maximum principal strain of fluid at the location of brine shrimp (●) and copepods (▲).

4.2 Upstream of cylinder

Figure 8 shows tracks of the (a) brine shrimp and (b) copepod upstream and downstream of the cylinder as determined from time sequence. For both zooplanktons, they appear to move steadily with the upstream flow, while their paths are

disorganized in the wake of the cylinder. However, the end-on views of the upstream paths for brine shrimp and copepods show a difference. In figure 8(a) insert, the brine shrimp appear to move steadily with the flow upstream. However, in figure 8(b), some copepods are observed to jump in the z-direction as they near the cylinder (marked by dotted ellipses). These are the copepods' escape responses, and they were observed to take place ~5-15 mm upstream of the cylinder. These copepod escape responses have higher velocity based on the spacing of neighboring spheres in the plotted tracks. We believe that these escaping copepods move far enough in the span wise direction that they are not re-circulated into the fluid directly behind the cylinder. Therefore, the lower number density in the wake is most likely attributed to the copepods responding to the sudden deceleration upstream of the cylinder.

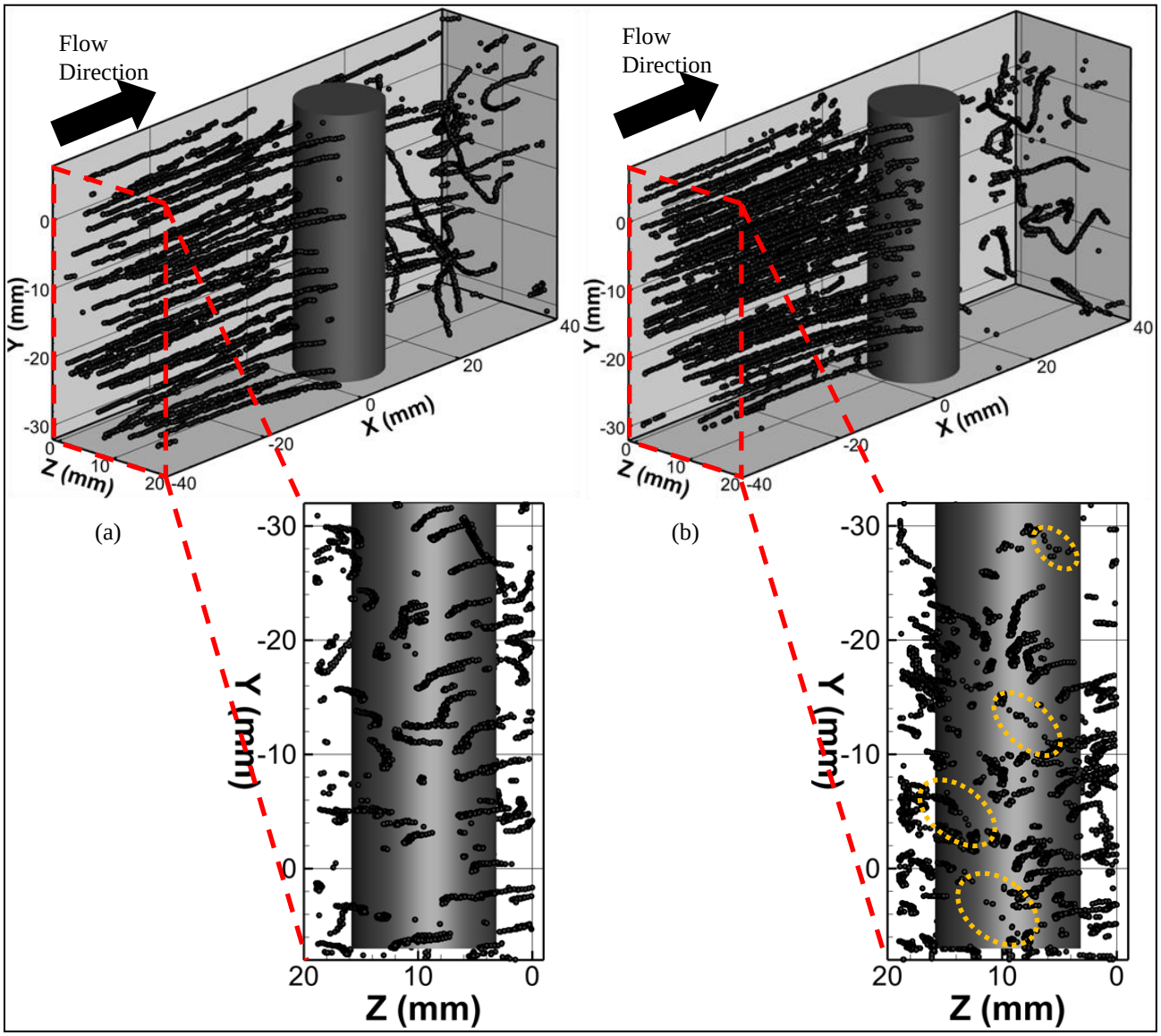

Figure 8 (a) Brine shrimp and (b) copepods showing their time series tracks (12 seconds) upstream and downstream of the cylinder with end-on views. Dotted ellipses show some instances of escape response by copepods when nearing the cylinder.

The velocity distribution upstream of the cylinder can be modeled using 2D potential flow theory. Consider a copepod approaching the cylinder on the stagnation streamline (see figure 9). Using 2D potential flow for cylinder in a uniform flow, we can obtain the velocity along the streamline as

$$v_r = -U_0\left(1 - \frac{{r_o}^2}{r^2}\right), \tag{5}$$

where U_0 is the velocity of freestream, r_0 is the radius of the cylinder and r is the point of interest in the fluid domain. Since the stagnation streamline does not have y-component velocity, equation (5) can be written in terms of x, where x originates at the cylinder center. The spatial gradient in x (i.e. $\partial v_r / \partial x$) can then be obtained as

$$\frac{\partial v_r}{\partial x} = -2U_o {r_0}^2 x^{-3} \quad (6)$$

Substituting the values r_0 = 6.35 mm, U_0 = 0.077 m/s and x = ~ - (5 to 15 + r_0) mm (based on the current experimental observation), we obtain $|\partial v_r / \partial x|$ = ~0.6 - 24 s^{-1}.

The maximum principal strain of the flow upstream of the cylinder was measured in the experiment. Figure 10 shows an averaged (time averaged for 12 seconds) velocity field measured upstream using the tomographic PIV. The contours show the maximum principal strain in the plane containing the stagnation streamline and parallel to x-y plane. From the contours, it appears that between x = -5 to -15 mm, the contours show values of maximum principal strain ranging from 0.5 – 7 s^{-1}. The measured values are generally less than the modeled values due to finite spatial resolution and viscosity. However, the minimum value obtained value from the model and experiment is of the same order as that reported by [5]. However, the large range of gradient values at which the copepod jumps, suggest that a simple threshold quantity may not be sufficient to model their behavior.

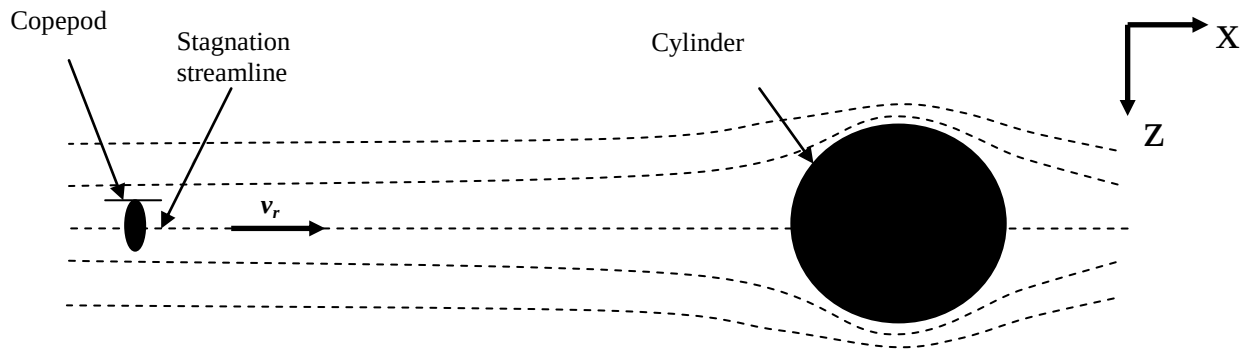

Figure 9 Schematic diagram of the copepod approaching the cylinder. Potential theory model is used, and the copepod is assumed to follow the stagnation streamline.

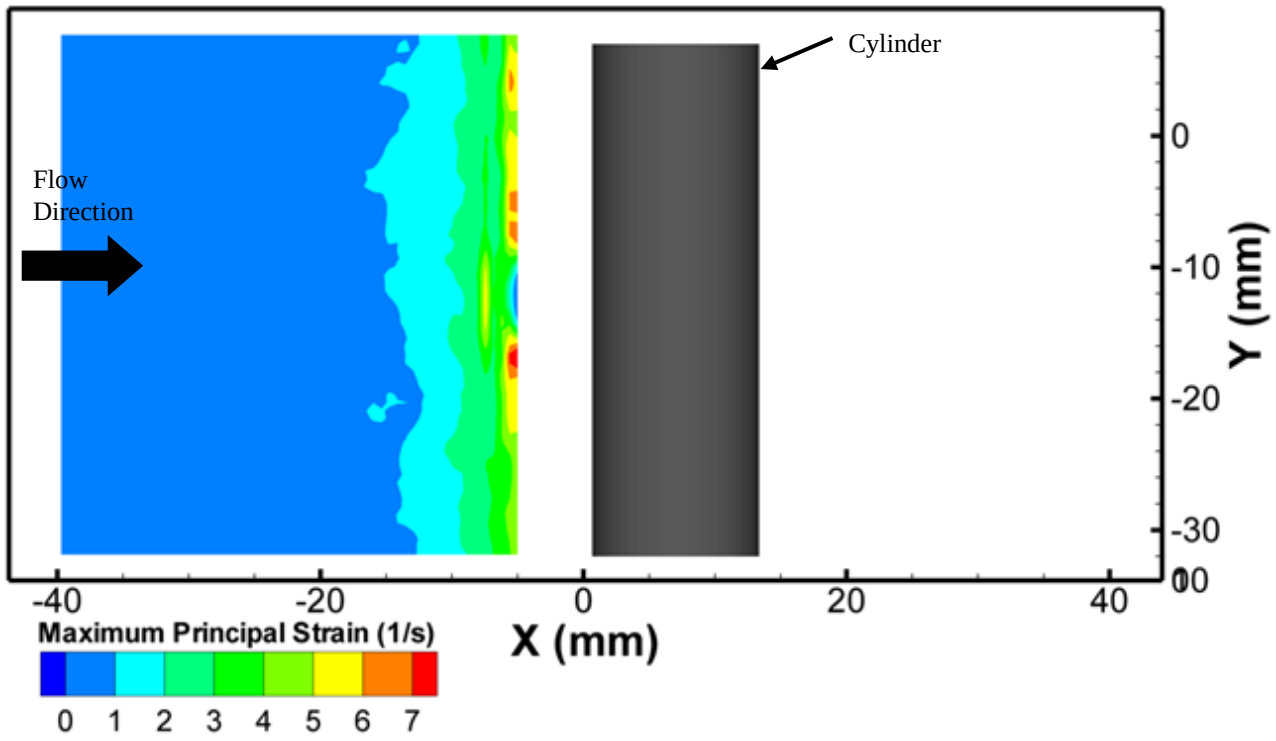

Figure 10 Contour of the maximum principal strain at the plane containing stagnation streamline and parallel to x-y plane.

5. SUMMARY

Simultaneous 3D PTV and infrared tomographic PIV have been successfully demonstrated to study zooplankton distribution. The system uses four cameras and an infrared laser for tomographic PIV, and two cameras and dark-field LED illumination for 3D PTV. With appropriate optical filters, algorithms, and PIV/PTV software, the system provides the volumetric flow velocity and the locations of the zooplankton simultaneously. In order to integrate the 3D PTV data and structured grid PIV data, a Taylor-series least-square technique is suggested. Results obtained indicate that this technique is able to measure zooplankton location, local fluid velocity and gradients in volumetric flow fields. This technique could be extended to other fluid dynamics problems including particle/turbulence interaction in three-dimensional environments.

The system was applied to study the distribution of brine shrimp and copepod downstream of a cylinder in cross flow. It was observed that the distribution of the two species differ behind the cylinder. This difference in distribution has been attributed to the response of copepods upstream (not downstream) of the cylinder. In the upstream location, the copepod senses a sudden deceleration and exhibits an escape with a z-component velocity. This suggests that fewer copepods eventually are drawn into the cylinder wake. Based on a potential flow model and experimental data, the escape response of copepods was found to be initiated for a relatively wide range of strain rate values. Furthermore, most copepods downstream of the cylinder were observed to remain in high strain rate regions without initiating any escape response. This suggests that the copepod-turbulence interaction is a complex problem which may not be modeled using a simple threshold quantity.

The results presented represent a first step toward improving the understanding of copepod response to flow disturbances in detail. Strain rate were the main quantities studied in this paper. Future work includes varying the cylinder diameter and flow velocity for various Stokes number and distribution of the maximum principal strain. Furthermore, analysis of additional parametric conditions that can be obtained from the time-evolving volumetric data, including acceleration, changes in strain rate per time, and vorticity.

Acknowledgments: This work is supported by NSF (IDBR - 0852875). We thank Professor Edward Buskey of University of Texas at Austin for providing the lab space and assistance with zooplankton collection and culture. We thank Dr Brad Gemmell for assistance with experiments.

REFERENCES

[1] Buskey EJ, Lenz PH and Hartline DK "Escape behavior of planktonic copepods in response to hydrodynamic disturbances: high speed video analysis" Marine Ecology Progress Series 235 (2002) pp. 135-146

[2] Yamazaki H and Squires KD “Comparison of oceanic turbulence and copepod swimming” Marine Ecology Progress Series 144 (1996) pp. 299-301

[3] Yen J, Lenz PH, Gassie DG and Hartline DK “Mechanoreception in marine copepods: electrophysiological studies on the first antennae” Journal of Plankton Research 14 (1992) pp. 495-512

[4] Strickler JR and Bal AK “Setae of the first antennae of the copepod *Cyclops scutifer* (Sars): Their structure and importance” Proceedings of the National Academy of Sciences 70 (1973) pp. 2656-2659

[5] Kiørboe T, Saiz E and Visser A "Hydrodynamic signal perception in the copepod *Acartia tonsa*" Marine Ecology Progress Series 179 (1999) pp. 97-111

[6] Woodson CB, Webster DR, Weissburg MJ and Yen J "Response of copepods to physical gradients associated with structure in the ocean" Limnology and Oceanography 50 (2005) pp. 1552-1564

[7] Catton KB, Webster DR and Yen J "The effect of fluid viscosity, habitat temperature, and body size on the flow disturbance of *Euchaeta*" Limnology and Oceanography: Fluids & Environment 2(2012) pp. 80-92

[8] Murphy DW, Webster DR and Yen J "A High-Speed Tomographic PIV Investigation of Plankton-Turbulence Interaction" 9th International Symposium on Particle Image Velocimetry, Kobe, Japan (2011)

[9] Murphy DW, Webster DR and Yen J "A High Speed Tomographic PIV System for Measuring Zooplankton Flow" Limnology and Oceanography: Methods 10 (2012) pp. 1096-1112

[10] Elsinga GE, Scarano F, Wieneke B and Oudheusden BW “Tomographic particle image velocimetry” Experiments in Fluids 41 (2006) pp. 933-947

[11] Maas HG, Gruen A and Papantoniou D "Particle tracking velocimetry in three-dimensional flows. Part 1 Photogrammetric determination of particle coordinates" Experiments in Fluids 15 (1993) pp. 133-146

[12] Wieneke B "Volume self-calibration for 3D particle image velocimetry" Experiments in Fluids 45 (2008) pp. 549-556

[13] Talapatra S and Katz J "Three-dimensional velocity measurements in a roughness sublayer using microscopic digital in-line holography and optical index matching" Measurement Science and Technology 24(2013) 024004

[14] Scarano F and Poelma C "Three-dimensional vorticity patterns of cylinder wakes" Experiments in Fluids 47 (2009) pp. 69-83

[15] Adrian RJ and Westerweel J "Particle Image Velocimetry" Cambridge University Press (2010)